nanomaterials

MDPI

Article

Preparation of Few-Layered MoS_2 by One-Pot Hydrothermal Method for High Supercapacitor Performance

Qingling Jia [1], Qi Wang [1], Lingshuai Meng [1], Yujie Zhao [1], Jing Xu [1], Meng Sun [1], Zijian Li [1], Han Li [1,*], Huiyu Chen [2,*] and Yongxing Zhang [1]

[1] Anhui Province Key Laboratory of Pollutant Sensitive Materials and Environmental Remediation, Anhui Province Key Laboratory of Intelligent Computing and Applications, Anhui Province Industrial Generic Technology Research Center for Alumics Materials, Huaibei Normal University, Huaibei 235000, China; zyx07157@mail.ustc.edu.cn (Y.Z.)

[2] School of Materials Science and Engineering, North University of China, Taiyuan 030051, China

* Correspondence: lh2017@mail.ustc.edu.cn (H.L.); hychen@nuc.edu.cn (H.C.)

Abstract: Molybdenum disulfide (MoS_2), a typical layered material, has important applications in various fields, such as optoelectronics, catalysis, electronic devices, sensors, and supercapacitors. Extensive research has been carried out on few-layered MoS_2 in the field of electrochemistry due to its large specific surface area, abundant active sites and short electron transport path. However, the preparation of few-layered MoS_2 is a significant challenge. This work presents a simple one-pot hydrothermal method for synthesizing few-layered MoS_2. Furthermore, it investigates the exfoliation effect of different amounts of sodium borohydride ($NaBH_4$) as a stripping agent on the layer number of MoS_2. Na^+ ions, as alkali metal ions, can intercalate between layers to achieve the purpose of exfoliating MoS_2. Additionally, $NaBH_4$ exhibits reducibility, which can effectively promote the formation of the metallic phase of MoS_2. Few-layered MoS_2, as an electrode for supercapacitor, possesses a wide potential window of 0.9 V, and a high specific capacitance of 150 F g^{-1} at 1 A g^{-1}. This work provides a facile method to prepare few-layered two-dimensional materials for high electrochemical performance.

Keywords: few layer; one-pot hydrothermal; MoS_2; exfoliation; supercapacitor performance

Citation: Jia, Q.; Wang, Q.; Meng, L.; Zhao, Y.; Xu, J.; Sun, M.; Li, Z.; Li, H.; Chen, H.; Zhang, Y. Preparation of Few-Layered MoS_2 by One-Pot Hydrothermal Method for High Supercapacitor Performance. *Nanomaterials* **2024**, *14*, 968. https://doi.org/10.3390/nano14110968

Academic Editor: Akihiko Fujiwara

Received: 26 April 2024
Revised: 30 May 2024
Accepted: 31 May 2024
Published: 2 June 2024

1. Introduction

In recent decades, it has been essential to develop a new generation of energy storage devices that are eco-friendly, sustainable, and capable of meeting the evolving energy demands [1–3]. Supercapacitors have attracted significant attention due to their superior power density and energy density, excellent cycle performance, and fast charge–discharge characteristics [4–6]. Supercapacitors can be divided into two categories (electrostatic double layer capacitors (EDLCs) and pseudocapacitors) based on the energy storage mechanisms [7]. Regarding EDLCs, the double-layer capacitor on the surface of the electrode material is formed through the effect of electrostatic force [8]. Pseudocapacitors store energy through rapid and reversible redox reactions or intercalation in the electrode material [9]. Thus, the selection of electrode materials is crucial for the performance of supercapacitors.

Molybdenum disulfide (MoS_2) is a two-dimensional material composed of molybdenum and sulfur atoms, belonging to the family of transition metal dichalcogenides [10,11]. In the structure of MoS_2, a Mo atomic layer is sandwiched between two sulfur atomic layers, forming a two-dimensional layered structure similar to graphene [12–14]. This layer structure imparts unique properties to MoS_2, such as excellent electrical, optical, and mechanical properties [15,16]. Within the interlayer space of molybdenum disulfide, electrolyte ions and molecules can diffuse, providing convenience for its electrochemical and catalytic applications [17–19]. The atomic-level thickness and two-dimensional structure of MoS_2 make it an ideal choice for researching and developing advanced materials and devices [20].

Specifically, the central Mo atoms exhibit oxidation states ranging from +2 to +6, creating an interlayer space that allows for the diffusion of electrolyte ions into the interlayers for Faraday reactions [21]. These distinctive features play a critical role in enhancing charge storage capabilities, ultimately enabling MoS_2 to achieve an impressive theoretical specific capacitance of approximately 1000 F g^{-1} [22]. The few-layered treatment of MoS_2 is able to expose more active sites, increase contact area with the electrolyte, and shorten the ion diffusion distance to further effectively enhance its electrochemical performance [23]. However, due to the challenges in preparing few-layered MoS_2 and the high technical requirements involved, the synthesis of few-layered MoS_2 faces significant hurdles.

In this work, few-layered MoS_2 is successfully prepared by the one-pot hydrothermal method with the effect of $NaBH_4$. Furthermore, the influence of different $NaBH_4$ dosages on few-layered MoS_2 is studied. The presence of few-layered MoS_2 after the $NaBH_4$ treatment is obtained using scanning electron microscopy (SEM) and transmission electron microscopy (TEM). MoS_2-0.3894 exhibits the excellent supercapacitor performance, including a wide potential window of 0.9 V and a high specific capacitance of 150 g^{-1} at 1 A g^{-1}. This work provides a simple way to achieve few-layered MoS_2, which has a significant impact on the development of two-dimensional layered materials.

2. Materials and Methods

2.1. Preparation of MoS_2 Nanosheets

First, 0.8225 g of sodium molybdate dihydrate ($Na_2MoO_4 \cdot 2H_2O$) and 0.7370 g of thioacetamide (C_2H_5NS) were dissolved in deionized water (25 mL) and stirred for 30 min. After the mixture was transferred to a Teflon-lined stainless-steel autoclave (100 mL), it was heated to 200 °C and kept for 20 h. The resulting product was washed several times with deionized water and ethanol, and then the sample was dried. Finally, the dried sample was ground into powder in a mortar to obtain MoS_2.

2.2. Preparation of MoS_2 with Different Amounts of NaBH4

First, 0.2595, 0.3894 and 0.5192 g of sodium borohydride ($NaBH_4$) was dissolved in homogeneous mixture composed of $Na_2MoO_4 \cdot 2H_2O$ and C_2H_5NS, and then stirred for 30 min. The rest of the operation process was the same as for the preparation of MoS_2 nanosheets. According to the various dosages of $NaBH_4$, the product samples are named MoS_2, MoS_2-0.2595, MoS_2-0.3894, and MoS_2-0.5192.

2.3. Material Characterizations

XRD patterns were collected on X-ray diffraction (PANalytical Empyrean, Bruker, Germany) with Cu K radiation (λ = 0.154 nm). Raman spectra were obtained by a spectrometer (TACHI Regulus8220) with 532 nm laser excitation. Materials nanostructure characterizations come from Field emission scanning electron microscope (FE-SEM, Hi-TACHI Regulus8220) and Energy-dispersive X-ray spectroscopy (EDX, Oxford EDX, with INCA software, INCA V7.5), transmission electron microscope (TEM, JEM-2100) with configured EDX.

3. Results and Discussion

As shown in Figure 1, the layered-material MoS_2 can be prepared into few-layered MoS_2 with the effect of $NaBH_4$. $NaBH_4$ is an excellent exfoliating and reducing agent. The alkali metal Na^+ ions have a significant exfoliating effect during synthesis processing. The group of BH_4^- exhibits strong reducing properties. In addition, various $NaBH_4$ have different effects on the exfoliation of MoS_2 layers [24,25]. The products are named MoS_2, MoS_2-0.2595, MoS_2-0.3894, and MoS_2-0.5192.

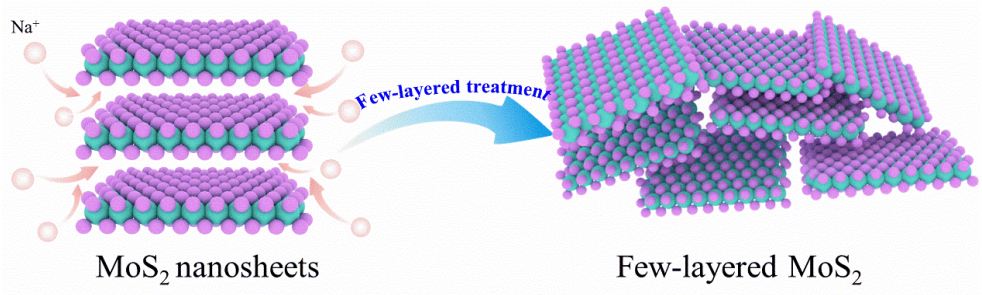

Figure 1. Schematic diagram of few-layered MoS_2 preparation.

The microscopic morphologies of all the samples obtained using scanning electron microscopy (SEM) are illustrated in Figure 2. As shown in the SEM images for MoS_2, MoS_2-0.2595, MoS_2-0.3894, and MoS_2-0.5192, it is clear that the nanoflowers of MoS_2 gradually disintegrated and agglomerated with an increase in the $NaBH_4$ dosage, which reflects the significant effect of $NaBH_4$ on MoS_2 morphology.

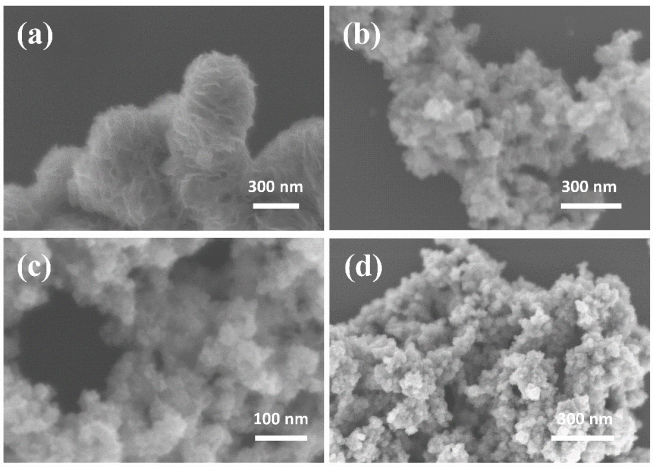

Figure 2. (**a**–**d**) The SEM images of MoS_2, MoS_2-0.2595, MoS_2-0.3894 and MoS_2-0.5192.

In order to clearly demonstrate this result, the morphology of MoS_2 treated with $NaBH_4$ was also observed using transmission electron microscopy (TEM). As shown in Figure 3a, the nanoflowers of MoS_2 are composed of a large number of nanosheets. Interestingly, for MoS_2-0.2595 and MoS_2-0.3894, the diameters of the nanoflowers are reduced, and their thickness is noticeably decreased. However, for MoS_2-0.5192, the nanosheets are much stacked, which resulted from the nanosheets of MoS_2 re-agglomerating after severe few-layered exfoliation. The layered structure of MoS_2 was observed using high-resolution transmission electron microscopy (HRTEM), and the characteristics of the multiple layers are shown in Figure 3e. As depicted in Figure 3f–h, MoS_2-0.2595 consists of approximately 5–6 layers, MoS_2-0.3894 contains around 3–4 layers, and MoS_2-0.5192 only exhibits 2 layers, indicating that $NaBH_4$ significantly influences the exfoliation process. Alkali metal Na^+ ions can intercalate into the interlayers of MoS_2 and achieve exfoliation of the layered materials during the hydrothermal process. The TEM results indicate that the amount of $NaBH_4$ is crucially related to the exfoliation effect. A significant amount of $NaBH_4$ can lead to evident fragmentation of MoS_2, ultimately resulting in its re-aggregation. The microstructure of materials plays a critical role in determining its electrochemical performance. Upon exfoliation of MoS_2, its increased interlayer spacing allows for improved ion transport and accessibility, leading to enhanced electrochemical reactions. Furthermore, the expanded specific surface area provides more active sites for electrochemical processes, ultimately boosting the material's performance in energy storage applications. Additionally, the presence of more defects can promote electrolyte penetration and enhance charge transfer

kinetics, further optimizing the electrochemical properties of electrode materials. However, the re-aggregation of few-layered MoS_2 can inhibit its electrochemical performance.

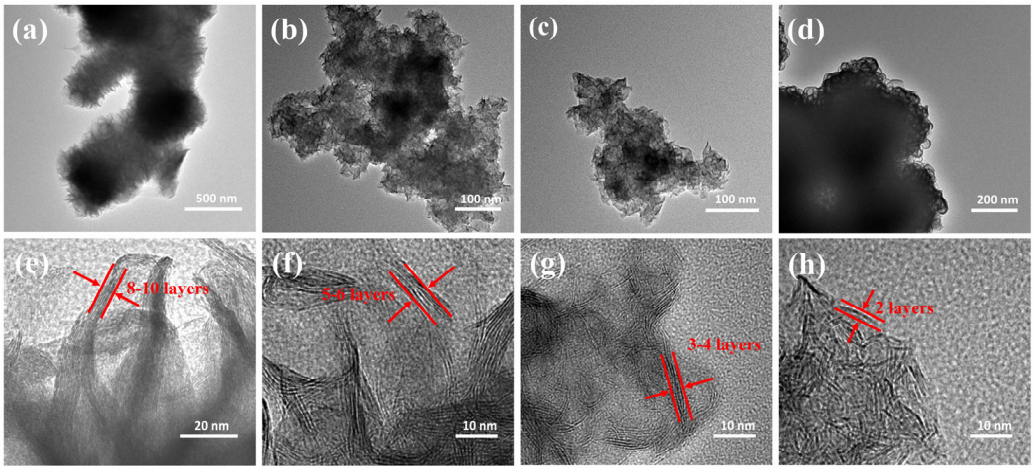

Figure 3. (**a**–**d**) The TEM images of MoS_2, MoS_2-0.2595, MoS_2-0.3894 and MoS_2-0.5192. (**e**–**h**) The HRTEM images of MoS_2, MoS_2-0.2595, MoS_2-0.3894 and MoS_2-0.5192.

To investigate the crystal structure of all samples, X-ray diffraction (XRD) was applied. As shown in Figure 4a, there are three characteristic peaks located at 9.3°, 32.2°, and 56.9°, which correspond to the (002), (100), and (110) planes of MoS_2 (JCPDS no. 37-1492), respectively [26]. The interlayer spacing was about 0.94 nm after calculation using the Bragg formula [27]. The wide interlayer spacing results from the intercalation of alkali metal Na^+ ions. On the one hand, the (002) peak of MoS_2 shifts from 9.4° to 8.2°, indicating the exfoliation of MoS_2 into few layers with the increase in the amount of $NaBH_4$. On the other hand, the (002) peak intensity of MoS_2 weakens after exfoliation, which resulted in defects that affected its X-ray diffraction and weaken the intensity of the characteristic peak. Large interlayer spacing and numerous defects can have a significant impact on the electrochemical performance of electrode materials. A large interlayer spacing helps to improve ion diffusion within the material, enhances electrolyte permeability, and facilitates more effective charge–discharge processes. An increased number of defects can provide additional active sites, thereby promoting ion and electron transfer, and enhancing the reactivity and electrochemical performance of the electrode [28]. Therefore, the few-layered treatment is often considered key technology for improving electrochemical performance.

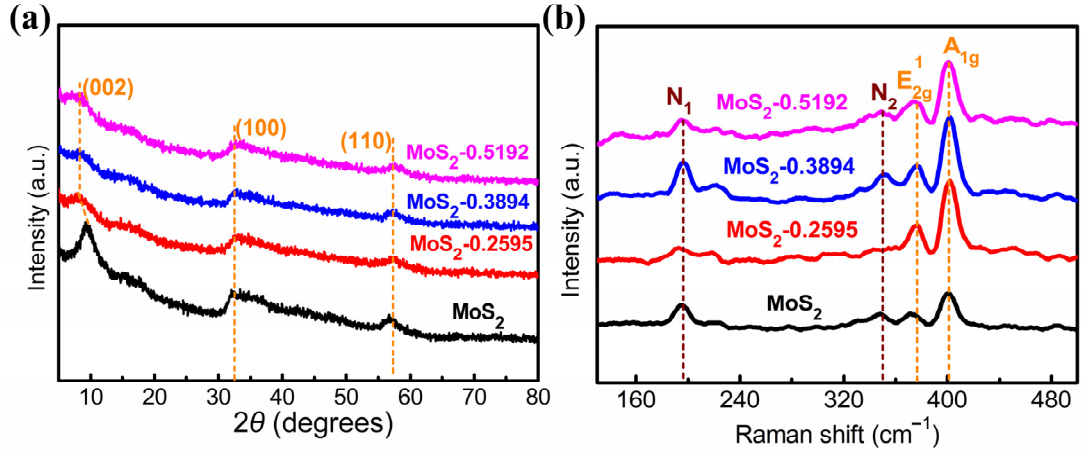

Figure 4. (**a**,**b**) The XRD patterns and Raman spectra of MoS_2, MoS_2-0.2595, MoS_2-0.3894, and MoS_2-0.5192.

Further phase analysis of MoS_2, MoS_2-0.2595, MoS_2-0.3894, and MoS_2-0.5192 was conducted using Raman spectroscopy, and the results are shown in Figure 4b, revealing characteristic peaks of 1T-MoS_2 and 2H-MoS_2 [29]. Two typical vibration modes of 2H-MoS_2, $E_{2g}{}^1$ and A_{1g}, can be observed at 377.0 cm^{-1} and 401.8 cm^{-1}, respectively. Interestingly, the characteristic peaks corresponding to 1T exhibited blue shifts toward the shortwave region. Peaks such as j_1, j_2, j_3, and E_{1g} shifted, accompanied by the appearance of two new peaks, N_1 at 195.2 cm^{-1} and N_2 at 352.0 cm^{-1}. The blue shift phenomenon often coincides with the generation of new peaks, highlighting structural changes within the material. According to the Raman spectroscopy results, the sample contained part of 1T-MoS_2. $NaBH_4$ provided additional electrons for the formation of 1T-MoS_2 due to its certain reduction properties during the exfoliation process of MoS_2. 1T-MoS_2 possesses high electrical conductivity, facilitating electron and ion transport to improve the response rate and charge–discharge efficiency of the electrode.

To display the supercapacitor performance of all samples, cyclic voltammetry (CV), galvanostatic charge–discharge (GCD), and electrochemical impedance spectroscopy (EIS) were evaluated using the three-electrode configuration. As shown in Figure 5a, the potential windows for MoS_2, MoS_2-0.2595, MoS_2-0.3894, and MoS_2-0.5192 are at 0.7, 0.8 and 0.9 V. Furthermore, as shown in Figure S1, the potential window for MoS_2-0.3894 is from −0.8 to 0.1 V, which implies that MoS_2-0.3894 has the largest potential window. Expanding the potential window not only enhances the capacitance capacity, contributing to the improved energy density and power density of supercapacitors, but also boosts response rates, enhancing the electrochemical kinetics performance of electrode materials. The expanded potential window was derived from the formation of the partial metallic phase of MoS_2 during the exfoliation process, thereby enhancing the conductivity, and contributing to the properties of electrode materials. Additionally, the areas surrounded by the CV curves represent the capacitance of the electrode materials. It is clear that MoS_2-0.3894 has the largest area of the CV curve compared to the other electrode materials, indicating the highest specific capacitance.

In order to more accurately reflect the specific capacitance, the GCD curves of each electrode are displayed in Figure 5b. There were some specific capacitances of 105.9, 148.2, 150 and 129.8 F g^{-1} for MoS_2, MoS_2-0.2595, MoS_2-0.3894 and MoS_2-0.5192, respectively, at a current density of 1 A g^{-1}. Obviously, the specific capacitance of MoS_2 was improved with the assistance of $NaBH_4$. As shown in Figure 5c, the rate performances of MoS_2, MoS_2-0.2595, MoS_2-0.3894, and MoS_2-0.5192 are displayed as 50.1%, 56.9%, 60.8%, and 49.3%, respectively, with a current density from 1 to 20 A g^{-1}. As the amount of $NaBH_4$ increased, the exfoliation of few-layered MoS_2 becomes more pronounced, leading to the formation of a larger specific surface area and an increased presence of metallic phase MoS_2, which enhanced the rate performance. However, in the case of MoS_2-0.5192, the re-stacking of exfoliated few-layered nanosheets resulted in a reduction in the specific surface area, impeding the diffusion of ions. As depicted in Table 1, following treatment with $NaBH_4$, the voltage window of MoS_2 was expanded, the specific capacitance of MoS_2 was enhanced, and the rate performance of MoS_2 was improved. These results adequately demonstrate that few-layered MoS_2 displays outstanding electrochemical performance.

Table 1. The potential windows, specific capacitance and rate performance of MoS_2, MoS_2-0.2595, MoS_2-0.3894, and MoS_2-0.5192.

Samples	MoS_2	MoS_2-0.2595	MoS_2-0.3894	MoS_2-0.5192
Potential window (V)	0.7	0.8	0.9	0.8
Specific capacitance (F g^{-1})	106	148.2	150	130
Rate performance (%)	50.1	56.9	60.8	49.3

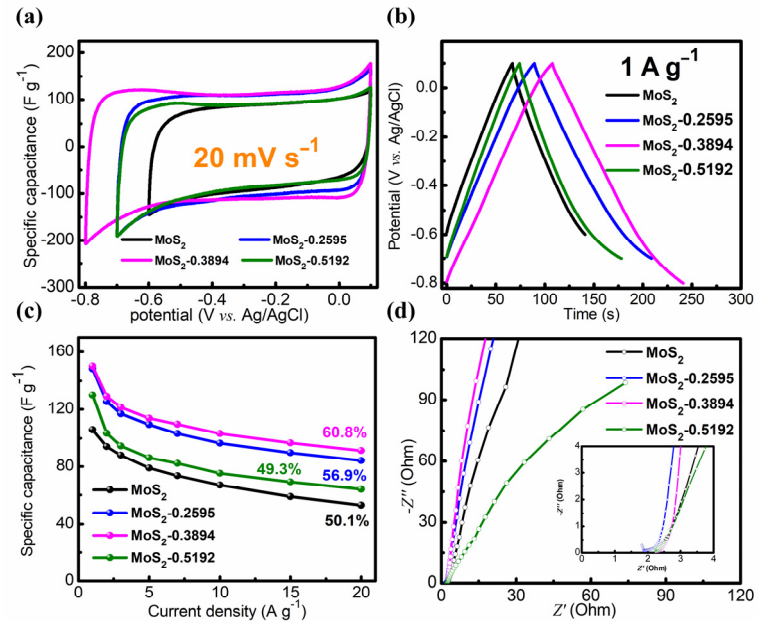

Figure 5. (**a**–**d**) The cyclic voltammetry (CV) curves, galvanostatic charge–discharge (GCD) curves, rate performance and electrochemical impedance spectroscopy (EIS) of MoS_2, MoS_2-0.2595, MoS_2-0.3894 and MoS_2-0.5192.

The EIS of each sample was measured, and the results are shown in Figure 5d. The EIS consists of high frequency and low frequency regions. In the high-frequency range, it typically represents the double-layer capacitance of the electrolyte at the electrode surface and the charge transfer process. In the low-frequency range, it usually represents the pseudocapacitance effect of the electrode material and the charge transfer process between the electrode and the electrolyte. MoS_2-0.3894 had the smallest radius, indicating the lowest charge transfer resistance in the high-frequency region. Furthermore, the slope of MoS_2-0.3894 was the biggest in the low frequency range compared to the other electrode materials, implying its capacitive-like behavior. Therefore, this indicates that MoS_2-0.3894 has low equivalent series resistance (ESR) and high conductivity.

As shown in Figure S2, the CV and GCD curves of MoS_2, MoS_2-0.2595, MoS_2-0.3894 and MoS_2-0.5192 are shown as a series of scan rates and current densities. It is clear that the CV curves are all rectangle-like, while the GCD curves are all triangle-like, which indicates the capacitive-like behavior of all electrodes. To determine the dynamics of each electrode, the b-value fitting of each electrode is shown. The CV curves of MoS_2-0.3894 electrode at various scan rates of 5, 10, 20, 30, 50, 70 and 100 mV s^{-1} were selected. The b-value fitting was calculated with the formula $i(v) = av^b$, where i represents the current density (A g^{-1}), v represents the scan rate (V s^{-1}), a and b are both constant, respectively [30]. When the b-value is close to 0.5, it indicates semi-diffusion-controlled behavior, whereas a b-value close to 1 indicates capacitance-controlled behavior [31]. According to Figure S3, the b-value had a range from 0.75 to 1, suggesting capacitive-like behavior for the MoS_2-0.3894 electrode. To clarify the contribution of capacitance behavior, the formula of $i(v) = k_1v + k_2v^{1/2}$ was used for fitting, where k_1v represents the contribution of capacitance behavior, while $k_2v^{1/2}$ represents the contribution of semi-diffusion behavior [32]. Figure S4 shows the fitting calculations of the capacitance contribution at different scan rates of 10, 20, 30, 50, 70, and 100 mV s^{-1}. Moreover, the capacitance contributions increased from 77.1% to 90.3% at scan rate of 10, 20, 30, 50, 70 and 100 mV s^{-1}, indicating high capacitance behavior.

4. Conclusions

In summary, few-layered MoS_2 was successfully prepared using the one-pot hydrothermal method with the assistance of $NaBH_4$. The exfoliation effects of different dosages of

$NaBH_4$ were also demonstrated in the results of the SEM and TEM images. Furthermore, a part of metallic phase MoS_2 was obtained in the process of exfoliation. In terms of the electrochemical performance, the optimal sample of MoS_2-0.3894 had a wide potential window of 0.9 V, the specific capacitance 150 F g^{-1} at 1 A g^{-1}, and a high rate performance of 60.8%. $NaBH_4$ plays an important role in the preparation of few-layered MoS_2. This work provides a simple and effective solution for the preparation of few-layered two-dimensional materials.

Supplementary Materials: The supporting information can be downloaded at: https://www.mdpi.com/article/10.3390/nano14110968/s1, Text S1: Experimental Section; Text S2: Electrochemical measurements and evaluations; Figure S1: The different potential windows of MoS_2-0.3894 for the cyclic voltammetry (CV) and galvanostatic charge–discharge (GCD) curves at a same scan rate of 20 mV s^{-1} and current density of 1 A g^{-1}; Figure S2: The CV and GCD curves of MoS_2-0.3894 at a series of scan rates and current densities; Figure S3: b-value for MoS_2-0.3894 electrode; Figure S4: CV partition analysis showing the capacitive contribution to the total current at select scan rates of 10, 20, 30, 50, 70 and 100 mV s^{-1}; Figure S5: Normalized contribution ratio of capacitive capacitance at different scan rates.

Author Contributions: Conceptualization, Q.J., H.L. and Y.Z. (Yongxing Zhang); methodology, H.L., H.C. and Y.Z. (Yongxing Zhang); software, Q.W., L.M., Y.Z. (Yujie Zhao) and J.X.; validation, H.L., H.C. and Y.Z. (Yongxing Zhang); formal analysis, H.L., H.C. and Y.Z. (Yongxing Zhang); investigation, Y.Z. (Yujie Zhao), J.X., M.S. and Z.L.; resources, H.L. and Y.Z. (Yongxing Zhang); data curation, Q.J. and H.L.; writing—original draft, Q.J. and H.L.; writing—review and editing, Q.J., H.L. and Y.Z. (Yongxing Zhang); visualization, Q.J., Q.W. and L.M; supervision, Y.Z. (Yongxing Zhang); project administration, H.L., H.C. and Y.Z. (Yongxing Zhang); funding acquisition, H.L. and Y.Z. (Yongxing Zhang). All authors have read and agreed to the published version of the manuscript.

Funding: This research was funded by the Key Natural Science Research Project for Colleges and Universities of Anhui Province (Grant No. 2022AH050384, KJ2021ZD0056), the University Enterprise Joint Research and Development Project (Grant No. 22100227, 22100229), the Excellent scientific research and innovation team of Education Department of Anhui Province (No. 2023AH010044), the University Synergy Innovation Program of Anhui Province (Grant No. GXXT-2023-098), the University Enterprise Joint Research and Development Project: Development of mod-ern spectral data mining and signal extraction techniques (Grant No. 2024340603000066).

Data Availability Statement: Data is contained within the article.

Conflicts of Interest: The authors declare no conflicts of interest.

References

1. Noori, A.; El-Kady, M.F.; Rahmanifar, M.S.; Kaner, R.B.; Mousavi, M.F. Towards establishing standard performance metrics for batteries, supercapacitors and beyond. *Chem. Soc. Rev.* **2019**, *48*, 1272–1341. [CrossRef] [PubMed]
2. Wang, Y.G.; Song, Y.F.; Xia, Y.Y. Electrochemical capacitors: Mechanism, materials, systems, characterization and applications. *Chem. Soc. Rev.* **2016**, *45*, 5925–5950. [CrossRef] [PubMed]
3. Maqsood, M.F.; Latif, U.; Sheikh, Z.A.; Abubakr, M.; Rehman, S.; Khan, K.; Khan, M.A.; Kim, H.; Ouladsmane, M.; Rehman, M.A.; et al. A comprehensive study of $Bi_2Sr_2Co_2O_y$ misfit layered oxide as a supercapacitor electrode material. *Inorg. Chem. Commun.* **2023**, *158*, 111487. [CrossRef]
4. Wei, Y.; Tang, B.; Liang, X.; Zhang, F.; Tang, Y. An ultrahigh-mass-loading integrated free-standing functional all-carbon positive electrode prepared using an architecture tailoring strategy for high-energy-density dual-ion batteries. *Adv. Mater.* **2023**, *35*, 2302086. [CrossRef] [PubMed]
5. Dubal, D.P.; Chodankar, N.R.; Kim, D.H.; Gomez-Romero, P. Towards flexible solid-state supercapacitors for smart and wearable electronics. *Chem. Soc. Rev.* **2018**, *47*, 2065–2129. [CrossRef] [PubMed]
6. Guo, T.Z.; Zhou, D.; Pang, L.X.; Sun, S.K.; Zhou, T.; Su, J.Z. Perspectives on working voltage of aqueous supercapacitors. *Small* **2022**, *18*, 2106360. [CrossRef] [PubMed]
7. Mu, H.C.; Wang, W.Q.; Yang, L.F.; Chen, J.; Li, X.W.; Yuan, Y.Z.; Tian, X.H.; Wang, G.C. Fully integrated design of intrinsically stretchable electrodes for stretchable. *Energy Storage Mater.* **2021**, *39*, 130–138. [CrossRef]
8. Lukatskaya, M.R.; Dunn, B.; Gogotsi, Y. Multidimensional materials and device architectures for future hybrid energy storage. *Nat. Commun.* **2016**, *7*, 12647. [CrossRef] [PubMed]
9. Sahoo, S.; Kumar, R.; Joanni, E.; Singh, R.K.; Shim, J.J. Advances in pseudocapacitive and battery-like electrode materials for high performance supercapacitors. *J. Mater. Chem. A* **2022**, *10*, 13190–13240. [CrossRef]

10. Heine, T. Transition metal chalcogenides: Ultrathin inorganic materials with tunable electronic properties. *Acc. Chem. Res.* **2015**, *48*, 65–72. [CrossRef]
11. Butler, S.Z.; Hollen, S.M.; Cao, L.Y.; Cui, Y.; Gupta, J.A.; Gutiérrez, H.R.; Heinz, T.F.; Hong, S.S.; Huang, J.X.; Ismach, A.F.; et al. Progress, Challenges, and opportunities in two-dimensional materials beyond graphene. *ACS Nano* **2013**, *7*, 2898–2926. [CrossRef] [PubMed]
12. Lin, L.X.; Lei, W.; Zhang, S.W.; Liu, Y.Q.; Wallace, G.G.; Chen, J. Two-dimensional transition metal dichalcogenides in supercapacitors and secondary batteries. *Energy Storage Mater.* **2019**, *19*, 408–423. [CrossRef]
13. Peng, L.L.; Zhu, Y.; Li, H.S.; Yu, G.H. Chemically integrated inorganic-graphene two-dimensional hybrid materials for flexible energy storage devices. *Small* **2016**, *12*, 6183–6199. [CrossRef] [PubMed]
14. Zhou, X.F.; Sun, H.N.; Bai, X. Two-dimensional transition metal dichalcogenides: Synthesis, biomedical applications and biosafety evaluation. *Front. Bioeng. Biotechnol.* **2020**, *8*, 236. [CrossRef] [PubMed]
15. Chen, J.L.; Walker, W.R.; Xu, L.Z.; Krysiak, O.; She, Z.M.; Pope, M.A. Intrinsic capacitance of molybdenum disulfide. *ACS Nano* **2020**, *14*, 5636–5648. [CrossRef] [PubMed]
16. Zhang, T.; Liu, Y.P.; Yu, J.; Ye, Q.T.; Yang, L.; Li, Y.; Fan, H.J. Biaxially strained MoS_2 nanoshells with controllable layers boost alkaline hydrogen evolution. *Adv. Mater.* **2022**, *34*, 2202195. [CrossRef] [PubMed]
17. Li, Y.; Wang, L.L.; Cai, T.; Zhang, S.Q.; Liu, Y.T.; Song, Y.Z.; Dong, X.R.; Hu, L. Glucose-assisted synthesize 1D/2D nearly vertical CdS/MoS_2 heterostructures for efficient photocatalytic hydrogen evolution. *Chem. Eng. J.* **2017**, *321*, 366–374. [CrossRef]
18. Nie, K.K.; Qu, X.Y.; Gao, D.W.; Li, B.J.; Yuan, Y.L.; Liu, Q.; Li, X.H.; Chong, S.K.; Liu, Z.Q. Engineering phase stability of semimetallic MoS_2 monolayers for sustainable electrocatalytic hydrogen production. *ACS Appl. Mater. Interfaces* **2022**, *14*, 19847–19856. [CrossRef]
19. Wan, Y.; Zhang, Z.Y.; Xu, X.L.; Zhang, Z.H.; Li, P.; Fang, X.; Zhang, K.; Yuan, K.; Liu, K.H.; Ran, G.Z.; et al. Engineering active edge sites of fractal-shaped single-layer MoS_2 catalysts for high-efficiency hydrogen evolution. *Nano Energy* **2018**, *51*, 786–792. [CrossRef]
20. Liu, M.Q.; Wang, J.A.; Klysubun, W.; Wang, G.G.; Sattayaporn, S.; Li, F.; Cai, Y.W.; Zhang, F.C.; Yu, J.; Yang, Y. Interfacial electronic structure engineering on molybdenum sulfide for robust dual-pH hydrogen evolution. *Nat. Commun.* **2021**, *12*, 5260. [CrossRef]
21. Yang, X.; Mao, J.J.; Niu, H.; Wang, Q.; Zhu, K.; Ye, K.; Wang, G.L.; Cao, D.X.; Yan, J. NiS_2/MoS_2 mixed phases with abundant active edge sites induced by sulfidation and graphene introduction towards high-rate supercapacitors. *Chem. Eng. J.* **2021**, *406*, 126713. [CrossRef]
22. Ma, G.F.; Peng, H.; Mu, J.J.; Huang, H.H.; Zhou, X.Z.; Lei, Z.Q. In situ intercalative polymerization of pyrrole in graphene analogue of MoS_2 as advanced electrode material in supercapacitor. *J. Power Sources* **2013**, *229*, 72–78. [CrossRef]
23. Wang, H.Y.; Ren, D.Y.; Zhu, Z.J.; Saha, P.; Jiang, H.; Li, C.Z. Few-layer MoS_2 nanosheets incorporated into hierarchical porous carbon for lithium-ion batteries. *Chem. Eng. J.* **2016**, *288*, 179–184. [CrossRef]
24. Qi, K.; Cui, X.Q.; Gu, L.; Yu, S.S.; Fan, X.F.; Luo, M.C.; Xu, S.; Li, N.B.; Zheng, L.R.; Zhang, Q.H.; et al. Single-atom cobalt array bound to distorted 1T MoS_2 with ensemble effect for hydrogen evolution catalysis. *Nat. Commun.* **2019**, *10*, 5231. [CrossRef] [PubMed]
25. Zhao, Y.; Liu, Y.C.; Liu, H.Q.; Kang, H.Y.; Cao, K.Z.; Wang, Q.H.; Zhang, C.L.; Wang, Y.J.; Yuan, H.T.; Jiao, L.F. Improved dehydrogenation performance of $LiBH_4$ by 3D hierarchical flower-like MoS_2 spheres additives. *J. Power Sources* **2015**, *300*, 358–364. [CrossRef]
26. Li, J.D.; Listwan, A.; Liang, J.X.; Shi, F.; Li, K.; Jia, J.P. High proportion of 1 T phase MoS_2 prepared by a simple solvothermal method for high-efficiency electrocatalytic hydrogen evolution. *Chem. Eng. J.* **2021**, *422*, 130100. [CrossRef]
27. Zhou, J.; Guo, M.; Wang, L.L.; Ding, Y.B.; Zhang, Z.Z.; Tang, Y.H.; Liu, C.B.; Luo, S.L. 1T-MoS_2 nanosheets confined among TiO_2 nanotube arrays for high performance supercapacitor. *Chem. Eng. J.* **2019**, *366*, 163–171. [CrossRef]
28. Gao, G.P.; Jiao, Y.; Ma, F.X.; Jiao, Y.L.; Waclawik, E.; Du, A.J. Charge mediated semiconducting-to-metallic phase transition in molybdenum disulfide monolayer and hydrogen evolution reaction in new 1T′ phase. *J. Phys. Chem. C* **2015**, *119*, 13124–13128. [CrossRef]
29. Hong, Z.A.; Hong, W.T.; Wang, B.C.; Cai, Q.; He, X.; Liu, W. Stable 1T-2H MoS_2 heterostructures for efficient electrocatalytic hydrogen evolution. *Chem. Eng. J.* **2023**, *460*, 141858. [CrossRef]
30. Feng, N.; Meng, R.J.; Zu, L.H.; Feng, Y.T.; Peng, C.X.; Huang, J.M.; Liu, G.L.; Chen, B.J.; Yang, J.H. A polymer-direct-intercalation strategy for MoS_2/carbon-derived heteroaerogels with ultrahigh pseudocapacitance. *Nat. Commun.* **2019**, *10*, 1372. [CrossRef]
31. Thiyagarajan, K.; Song, W.J.; Park, H.; Selvaraj, V.; Moon, S.; Oh, J.; Kwak, M.J.; Park, G.; Kong, M.; Pal, M.; et al. Electroactive 1T-MoS_2 fluoroelastomer ink for intrinsically stretchable solid-state in-plane supercapacitors. *ACS Appl. Mater. Interfaces* **2021**, *13*, 26870–26878. [CrossRef] [PubMed]
32. Tiwari, P.; Janas, D.; Chandra, R. Self-standing MoS_2/CNT and MnO_2/CNT one dimensional core shell heterostructures for asymmetric supercapacitor applications. *Carbon* **2021**, *177*, 291–303. [CrossRef]